



Green synthesis and electrochemical performances of ZnO/graphene nanocomposites

Yunfu Liu¹ · Guohui Liu¹

Received: 22 December 2021 / Revised: 14 March 2022 / Accepted: 11 April 2022 / Published online: 12 May 2022
© The Author(s), under exclusive licence to Springer-Verlag GmbH Germany, part of Springer Nature 2022

Abstract

ZnO/graphene nanocomposites were prepared for supercapacitance materials through a simple two-step process involving chemical oxidation of flake graphite powders and solvothermal synthesis of ZnO/graphene nanocomposites in ethanol. The structure, Brunauer-Emmett-Teller surface area, composition, and morphology of the as-prepared materials were characterized by X-ray diffraction, N₂ adsorption/desorption analysis, Fourier transform infrared spectroscopy, and transmission electron microscopy. Results showed that the ZnO nanorods had wurtzite structure and were successfully loaded on the graphene sheets. The electrochemical properties of ZnO/graphene nanocomposites formed by different masses of graphite oxide to zinc acetylacetonate were evaluated by means of cyclic voltammetry and galvanostatic charge-discharge studies. The nanocomposite prepared with graphite oxide (60 mg) and zinc acetylacetonate (15 mg) showed a high specific capacitance of 188 Fg⁻¹ at a current density of 0.1 Ag⁻¹ in the 6 M KOH solution and better long-term stability along with 98.25% of its initial capacitance after 1500 cycles at 1.2 Ag⁻¹.

Keywords Graphene · ZnO · Solvothermal · Supercapacitor

Introduction

Supercapacitors are considered as striking candidates for energy storage due to simple principle, long cyclic life, and quick charging/discharging [1]. Its performances highly depend on the properties of electrode materials. Comparing with traditional porous carbon materials, graphene (GH) has higher specific capacitance and power density because of its faster electron mobility ($\geq 15,000 \text{ cm}^2 \text{ V}^{-1} \text{ s}^{-1}$) [2] and larger surface area ($2675 \text{ m}^2 \text{ g}^{-1}$) [3]. As a promising metal oxide, ZnO is widely recognized as a battery active material with superior energy density of 650 Ahg^{-1} and has good electrical conductivity (up to 230 Scm^{-1}) [4]. Hence, the combination of GH with ZnO as electrodes may result in improved supercapacitor performance [5–7].

In recent years, a number of methods have been adopted to prepare ZnO/GH nanocomposites. Kumar et al. [8] have carried out one-step synthesis of reduced graphene oxide

nanosheets anchored ZnO nanoparticles via microwave irradiation. The obtained nanocomposite had a specific capacitance of 102.4 Fg^{-1} at the scan of 30 mVs^{-1} . Halderal et al. [9] have successfully fabricated nano-ZnO@reduced graphene oxide composite by using a supercritical fluid (ScCO_2) to separate graphene oxide nanosheets and disperse ZnO nanoparticles in between. The composite could deliver a high specific capacitance of 303 Fg^{-1} at 5 mVs^{-1} . Zhang et al. [10] reported that graphite oxide (GO) produced by a modified Hummers method was reduced GH with hydrazine and ZnO was deposited on GH by ultrasonic spray pyrolysis. The as-prepared material exhibited a capacitance value of 11.3 Fg^{-1} at 50 mVs^{-1} . By chemical vapor deposition and hydrothermal method, Li et al. [11] have made the porous graphene/ZnO nanorod composite networks with a higher specific capacitance of 554.23 Fg^{-1} at 5 mVs^{-1} . Samuel et al. [12] have obtained a binder-free nanocomposite consisting of ZnO nanoparticles grown directly on graphene sheets by electrospraying. The composite showed good cycle stability, retaining 90% of the initial capacitance after 1000 cycles. Bu et al. [13] have employed the sol-gel deposition method to produce ZnO/reduced graphene oxide nanocomposite film as supercapacitor material by using an integration of zinc acetate and graphite. Subramani et al. [14] have

✉ Yunfu Liu
liuyunfu@usth.edu.cn

¹ School of Environmental and Chemical Engineering, Heilongjiang University of Science and Technology, Harbin 150022, People's Republic of China

synthesized the ZnO nanoflowers/reduced graphene oxide nanocomposite by direct chemical decomposition of zinc hexacyanoferrate over reduced graphene oxide nanosheets and achieved a specific capacitance of 203 Fg^{-1} at 1 Ag^{-1} . Du et al. [15] have prepared the ZnO nanoflakes/graphene hybrid film through filtration self-assembly and thermal reduction process, which exhibited a maximum capacitance value of 167.2 Fg^{-1} at 5 mVs^{-1} . In comparison with the above ways, the solvothermal method is a promising route for fabricating ZnO-graphene nanocomposites, owing to its advantages of environment friendly, simple operation, and high product purity. By a liquid phase exfoliation and solvothermal synthesis method, Ezeigwe et al. [16] have developed graphene/ZnO nanocomposites for supercapacitor electrodes that attained a capacitance value of 236 Fg^{-1} at 10 mVs^{-1} . Du et al. [17] pointed out that the graphene-ZnO nanocomposites synthesized through a one-step hydrothermal approach and achieved an enhanced specific capacitance of 118 Fg^{-1} at 0.1 Ag^{-1} . Therefore, we have also used the facile method to prepare ZnO/GH nanocomposites for supercapacitors.

In this work, a high specific capacitance of ZnO/GH-5 nanocomposites ($\sim 188 \text{ Fg}^{-1}$) was prepared by solvothermal route in an ethanol solution due to its lower-price and non-toxic. The influences of different mass ratios of GO to zinc acetylacetonate ($\text{Zn}(\text{C}_5\text{H}_7\text{O}_2)_2$) for preparing ZnO/GH nanocomposites and on electrochemical performances of these composites have been explored. The as-synthesized materials were investigated by X-ray diffraction (XRD), Fourier transform infrared spectroscopy (FT-IR), Raman spectroscopy, field emission scanning electron microscopy (FESEM), transmission electron microscopy (TEM), cyclic voltammetry (CV), electrochemical impedance spectroscopy (EIS), and galvanostatic charge-discharge cycling techniques (GCD), respectively.

Experimental

GO was synthesized by a modification of the Hummers method. Concentrated H_2SO_4 (70 mL) was added in the mixture of flake graphite (FG) powder (3.0 g, 99.9% carbon purity) and NaNO_3 (1.5 g) in the flask, then cooled in an ice bath, and stirred for 30 min. KMnO_4 (9.0 g) was gradually placed into the mixed solution and its temperature was controlled under 293 K. After stirring for 2 h in the ice bath, the mixed solution was transferred into the water bath and kept at 308 K for 1 h. Deionized water (140 mL) was followed to add into the mixture and caused its temperature slowly up to 371 K, maintaining at the temperature for 1 h. Then, the mixture was put into 420 mL warm water (323 K) and treated with 30 mL of 30 wt% H_2O_2 . Finally, the resulting mixture was separated by the high-speed centrifugation

(8000 Rpm), washed with 5 wt% HCl solution and water respectively, and dewatered by vacuum drying at 323 K for 96 h.

GO (60 mg) was dispersed in ethanol (60 mL) by sonication for 1 h. Subsequently, $\text{Zn}(\text{C}_5\text{H}_7\text{O}_2)_2$ (reagent grade 99.9%) was added into the solution with different masses (200 mg, 100 mg, 50 mg, 25 mg, and 15 mg) to synthesize the ZnO/GH nanocomposites, respectively. After continued to ultrasonic treatment for 3 h again, the obtained suspension was sealed into a teflon-lined autoclave (100 mL) and heated at 433 K for 12 h. The as-produced nanocomposite was filtered, washed with ethanol solution, and vacuum-dried at 338 K for 24 h. For comparison with these samples, pure ZnO and GH had been also prepared by the same method. Table 1 shows detailed information of the different masses of GO and $\text{Zn}(\text{C}_5\text{H}_7\text{O}_2)_2$ which were used to prepare the ZnO/GH nanocomposites.

The structures of the samples were investigated using a Rigaku D/MAX-RB X-ray diffractometer with $\text{Cu K}\alpha$ radiation ($\lambda=0.15406 \text{ nm}$). FT-IR spectra were recorded in KBr pellets on a Bruker TENSOR-27 spectrometer. Raman spectra were recorded by a Jobin Yvon HR800 Raman spectrometer at 458 nm. The morphologies of samples were observed by FESEM (FEI, Quanta 200F) and TEM (FEI, Tecnai F20) operated at 200 kV. The element compositions of samples were determined by an energy dispersive X-ray analysis spectroscopy (EDAX). The surface areas and porous structures of as-prepared GH and ZnO/GH nanocomposite were examined by physical adsorption of N_2 (ASAP 2020, Micromeritics Inc.) at 77 K.

The test electrodes were prepared by mixing 80 wt% of as-prepared materials, 10 wt% of carbon black, and 10 wt% of polyvinylidene fluoride as a binder. NMP was added to the mixture as solvent to get homogeneous slurry. Then the slurry was pasted onto nickel foam current collectors (1 cm^2), followed by vacuum drying at 378 K for 24 h. Activated carbon electrodes were prepared as the counter electrode by the above method.

Electrochemical measurements were performed, using three-electrode system with the test electrode, counter electrode, and Hg/HgO electrode as the reference electrode in

Table 1 Different mass ratios of GO to $\text{Zn}(\text{C}_5\text{H}_7\text{O}_2)_2$ used to produce ZnO/graphene nanocomposites

Name of sample	Mass of graphite oxide (mg)	Mass of zinc acetylacetonate (mg)
ZnO/GH-1	60	200
ZnO/GH-2	60	100
ZnO/GH-3	60	50
ZnO/GH-4	60	25
ZnO/GH-5	60	15

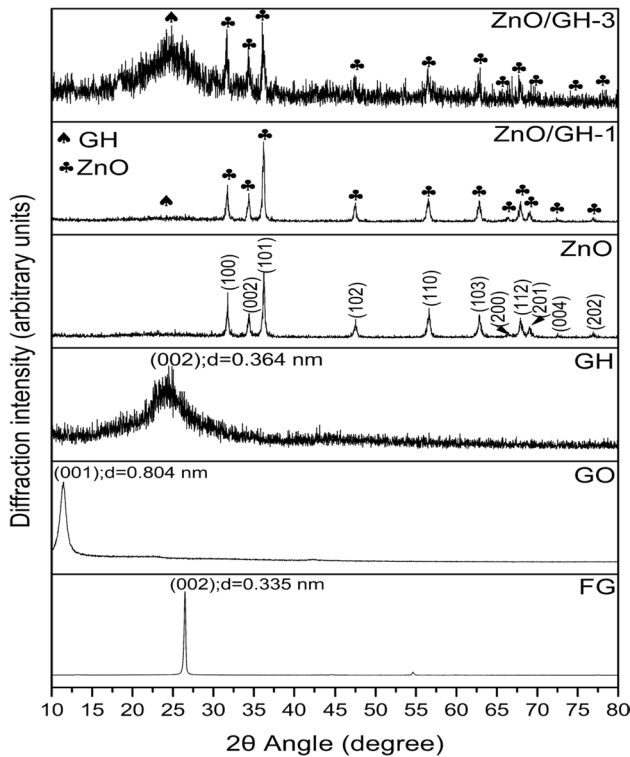


Fig. 1 XRD patterns of FG, GO, GH, ZnO, and ZnO/graphene nanocomposites

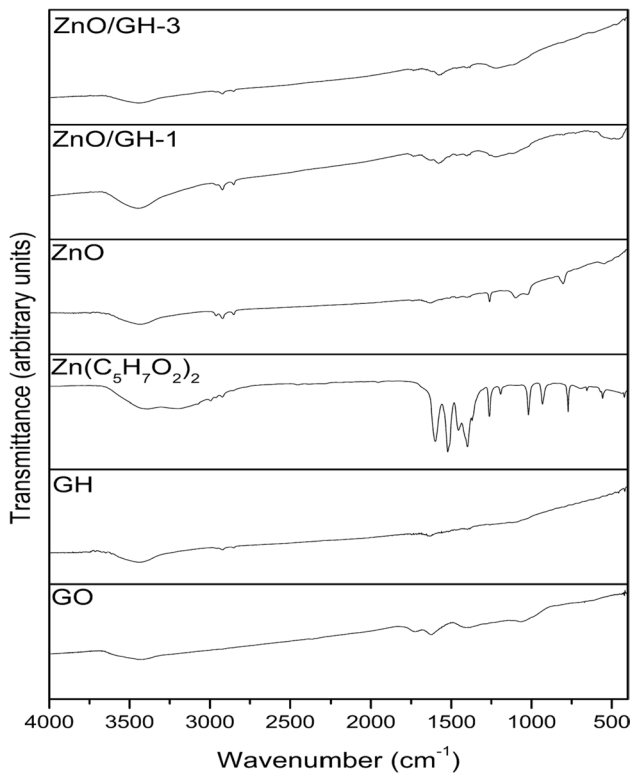


Fig. 2 FT-IR spectra for GO, GH, $Zn(C_5H_7O_2)_2$, ZnO, and ZnO/GH nanocomposites

the 6 M KOH solution at room temperature. CV was investigated on a CHI 604E electrochemical workstation (CHI, Shanghai China) and GCD curves were tested by a Neware battery testing workstation (Neware, Shengzhen China). EIS were measured in the frequency range of 100 kHz–0.01 Hz at open circuit potential with an ac perturbation of 5 mV by a PARSTAT 2273 advanced electrochemical system (Princeton Applied Research, USA).

Result and discussion

Figure 1 shows XRD patterns of FG, GO, GH, ZnO, and ZnO/GH nanocomposites. FG has a typical peak at 26.56° , corresponding to the (002) interlayer spacing, $d_{002}=0.335$ nm. When FG is oxidized through concentrated H_2SO_4 and $KMnO_4$, the Bragg (002) peak has vanished and a characteristic (001) peak of GO arises at 11.40° , with d-spacing of expansion to 0.804 nm. After solvothermal reduction at 433 K for 12 h, a majority of oxygen-containing groups of GO have been removed and its π -bonding restored to provide GH. The (002) peak of GH exhibits a broad peak at 24.38° with $d_{002}=0.364$ nm, which is larger than that of FG, due to forming the disordered layer stacking of GH with a small amount of residual oxygen functional groups [18].

From the XRD pattern of as-prepared ZnO, the peaks of 31.72° , 34.36° , 36.21° , 47.47° , 56.59° , 62.85° , 66.39° ,

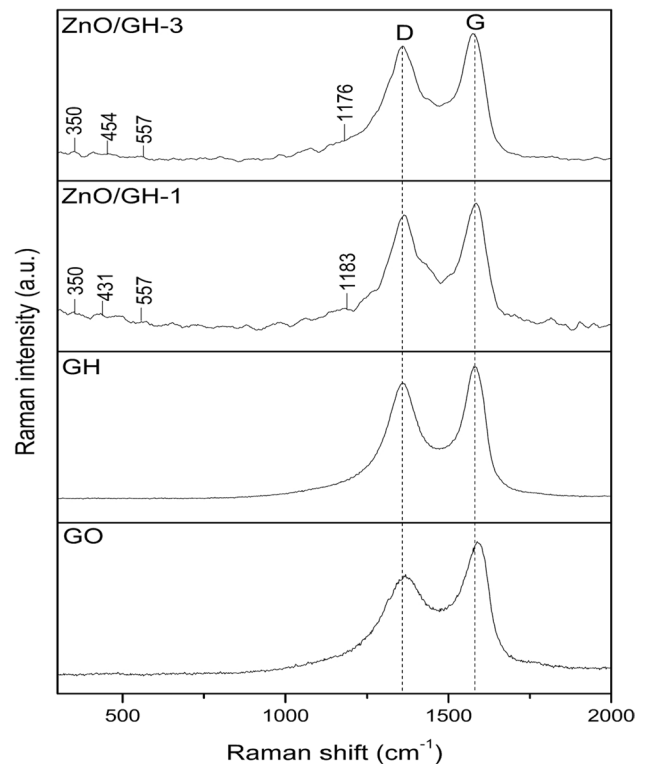


Fig. 3 Raman spectra for GO, GH, and ZnO/GH nanocomposites

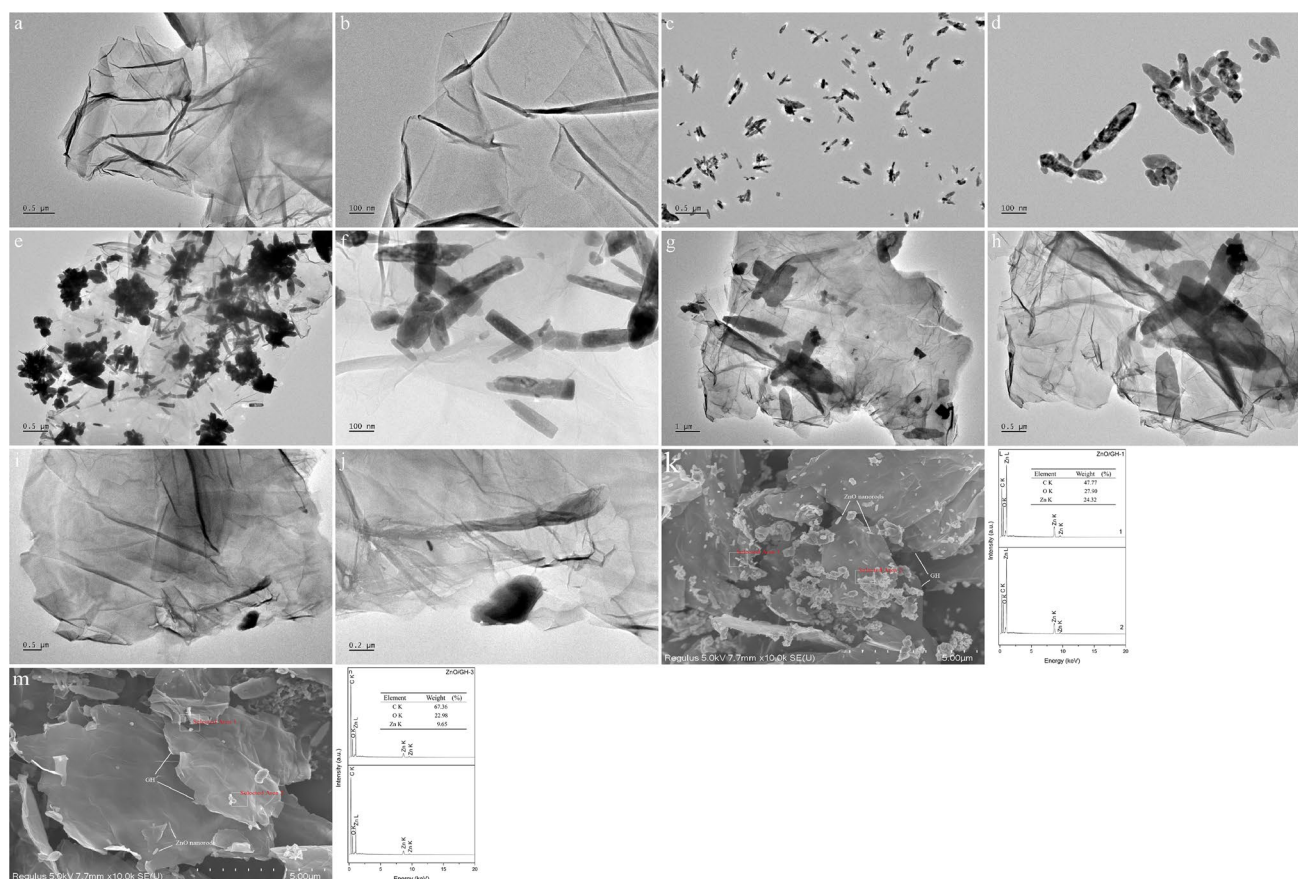


Fig. 4 TEM images of GH (a, b), ZnO (c, d), ZnO/GH nanocomposites (e–j); FESEM images (k, m) and EDAX spectra (l, n) of ZnO/GH nanocomposites

67.90°, 69.07°, 72.53°, and 76.94° are in good accordance with the standard values of ZnO (JCPDS 36-1451) [3]. It can also be seen that the XRD data of ZnO/GH-1 and ZnO/GH-3 nanocomposites possess both the (002) peak of GH and similar peaks of pure ZnO. However, the GH-related peak becomes weak because the ZnO cover the surfaces of GH in the nanocomposites and give strong diffraction peaks. In addition, no peaks corresponding to impurities are found, implying that the as-obtained nanocomposites are of high purity.

The FT-IR spectra of GO, GH, $\text{Zn}(\text{C}_5\text{H}_7\text{O}_2)_2$, ZnO, ZnO/GH-1, and ZnO/GH-3 nanocomposites are shown in Fig. 2. The typical absorption bands of GO were observed at around 1073, 1277, 1404, 1618, 1752, and 3413 cm^{-1} , corresponding to alkoxy C–O stretch, epoxy C–O stretch, aromatic C=C stretch, carboxyl O–H bend, carboxyl and carbonyl C=O stretch, and O–H stretch of adsorbed water molecules, respectively [19, 20]. After the solvothermal reaction, the O–H vibration bands and C–O and C=O stretching bands completely disappeared and carbonyl group attenuated, which the critical dissociation temperature of carbonyl group is higher than that of carboxyl and hydroxyl groups

according to the paper of Gao et al. [21]. This indicates that the GO has successfully been reduced to GH.

From the FT-IR spectrum of $\text{Zn}(\text{C}_5\text{H}_7\text{O}_2)_2$, it was observed that the absorption bands of deformation vibration, rocking vibration, and bending vibration of C–H in methyl group at around 1403, 1017, and 773 cm^{-1} , respectively. There are the absorption bands of Zn–O stretching vibration, C–C stretching vibration, C–C bending vibration, C=C stretching vibration, C=O stretching vibration, and O–H vibration at approximately 556, 1190, 1262, 1520, 1602, and 3393 cm^{-1} , respectively. The formation of ZnO is represented by the Zn–O stretching vibration at 549 cm^{-1} . The bands centered at 3433 and 1622 cm^{-1} in spectrum of ZnO are due to the stretching and bending modes of the water molecules adsorbed on ZnO, respectively. In the meanwhile, the disappearance of most infrared absorption bands reveals that the decomposition of $\text{Zn}(\text{C}_5\text{H}_7\text{O}_2)_2$ is almost complete [22, 23]. In the case of ZnO/GH-1 and ZnO/GH-3 nanocomposites, the absorption peaks at around 534, 1587, and 3434 cm^{-1} disclose the stretching vibration of Zn–O and skeletal vibration of GH and H_2O (moisture) adsorbed on samples,

respectively [24]. Therefore, these results indicate the formation of ZnO on GH matrix.

In the Raman spectra of GO, GH, ZnO/GH-1, and ZnO/GH-3 nanocomposites (Fig. 3), two prominent peaks of D and G bands locate at around 1368 and 1585 cm^{-1} , respectively. The D band originates from the breathing mode of κ -point phonons of A_{1g} symmetry, while G band is due to the first order scattering mode of the E_{2g} phonon of sp^2 domain of the carbon atom [25]. The D/G intensity (I_D/I_G) ratio is a measure of the concentration of defects in GH [26]. The I_D/I_G ratios of GO, GH, ZnO/GH-1, and ZnO/GH-3 nanocomposites are 0.7574, 0.8861, 0.8826, and 0.9001, respectively. Compared to that of GO, the increased I_D/I_G ratios of other samples indicate that some oxygen atoms are eliminated to generate more defects and a great deal of smaller graphitic domains are formed during the reduction of exfoliated GO [27, 28]. In addition, several peaks appear in the Raman spectra of ZnO/GH-1 and ZnO/GH-3 nanocomposites. The ones located at about 557 cm^{-1} and 1183 cm^{-1} are ascribed to the LO phonon of A_1 mode of ZnO, whereas the others observed at around 431 cm^{-1} and 350 cm^{-1} correspond to the vibration modes of E_2 and multiple-phonon scattering processes of ZnO, respectively [29, 30]. The Raman spectra reveal that ZnO/GH nanocomposites have been generated, which is in good agreement with the XRD results (Fig. 1).

The morphology differences of GH, ZnO, and ZnO/GH nanocomposites were observed in TEM images. Figure 4a and b exhibit that the as-prepared GH is a transparent, curled, and partially folded few-layer GH. As seen from in Fig. 4c and d, the most pure ZnO are rod-shaped and agglomerated. The lengths of these nanorods are in the range of approximately 50 to 200 nm. Based on the TEM images and XRD results, it can be concluded that the ZnO nanorods are single-crystalline wurtzite structure. From the TEM images (Fig. 4e–j) of ZnO/GH-1, ZnO/GH-3, and ZnO/GH-5 nanocomposites, the amount of ZnO nanorods was found to be decreased by a decrease in the loading mass of Zn precursor. Figure 4e and f depict that the ZnO nanorods produced from $\text{Zn}(\text{C}_5\text{H}_7\text{O}_2)_2$ (200 mg) have been formed a large number of heavy clusters non-uniformly dispersed on the surfaces of GH. On the contrary, the few ZnO nanorods made through $\text{Zn}(\text{C}_5\text{H}_7\text{O}_2)_2$ (15 mg) are scatteredly decorated on the surfaces of GH, as shown in Fig. 4i and j.

To further investigate the morphologies and element compositions of materials obtained, FESEM equipped with EDAX was performed on ZnO/GH-1 (Fig. 4k and l) and ZnO/GH-3 nanocomposites (Fig. 4m and n). As shown in Fig. 4k and m, GH exhibits sheet-like morphology without apparent stacking order and has wrinkles on the edge of the GH. The numerous ZnO nanorods are closely anchored onto the planes and edges of GH. In some regions, the agglomeration of ZnO nanorods could be found also. Compared to

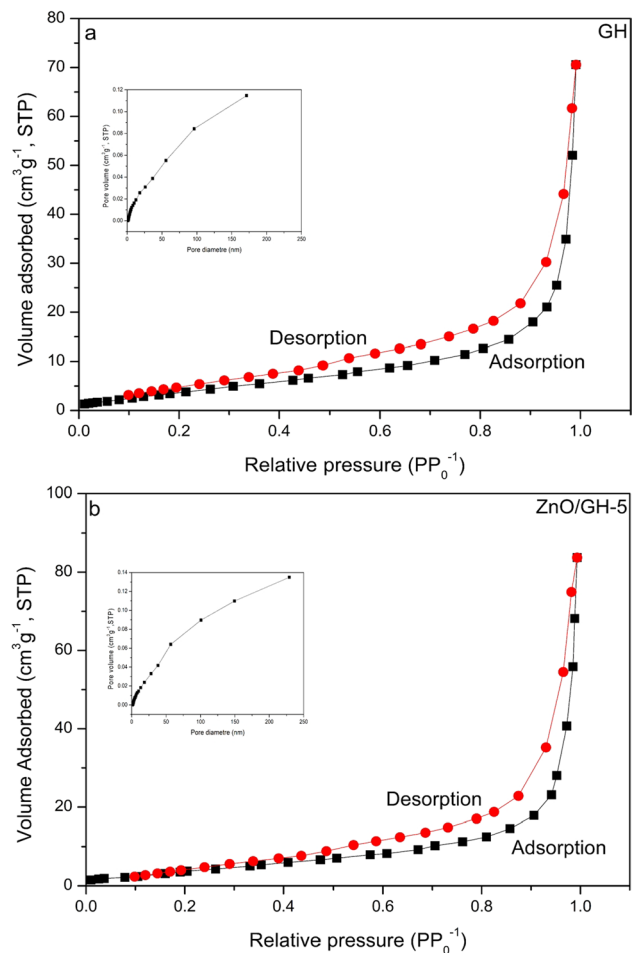


Fig. 5 The N_2 adsorption/desorption isotherms of GH (a) and ZnO/GH nanocomposites (b)

the ZnO/GH-1 and ZnO/GH-3 nanocomposites, more ZnO nanorods will be generated on the surfaces and edges of GH with the increase of Zn precursor addition. The peaks of C, O, and Zn in the EDAX spectra (Fig. 4l and n) display the presence of carbon, oxygen, and zinc elements on the surfaces of ZnO/GH nanocomposites only, therefore proving the purity of the as-synthesized nanocomposites.

Figure 5 displays the N_2 adsorption/desorption isotherms and Barrett-Joyner-Halenda (BJH) pore-size distributions of the as-prepared GH and ZnO/GH-5 nanocomposites. The isotherms of samples all exhibit type III with H3 hysteresis loops in the IUPAC classification [31], indicating their mesoporous structures with the slit-shaped pores formed by the aggregated graphene slices or ZnO nanorods, in accordance with the average pore sizes of GH (20.14 nm) and ZnO/GH-5 nanocomposites (24.35 nm). The BET surface of ZnO/GH-5 sample ($33.08 \text{ m}^2\text{g}^{-1}$) is bigger than that of GH ($30.32 \text{ m}^2\text{g}^{-1}$). Because the conversion of GO into GH by solvothermal reduction needs a longer time in a weaker reductant of ethanol solution, the graphene sheets might be

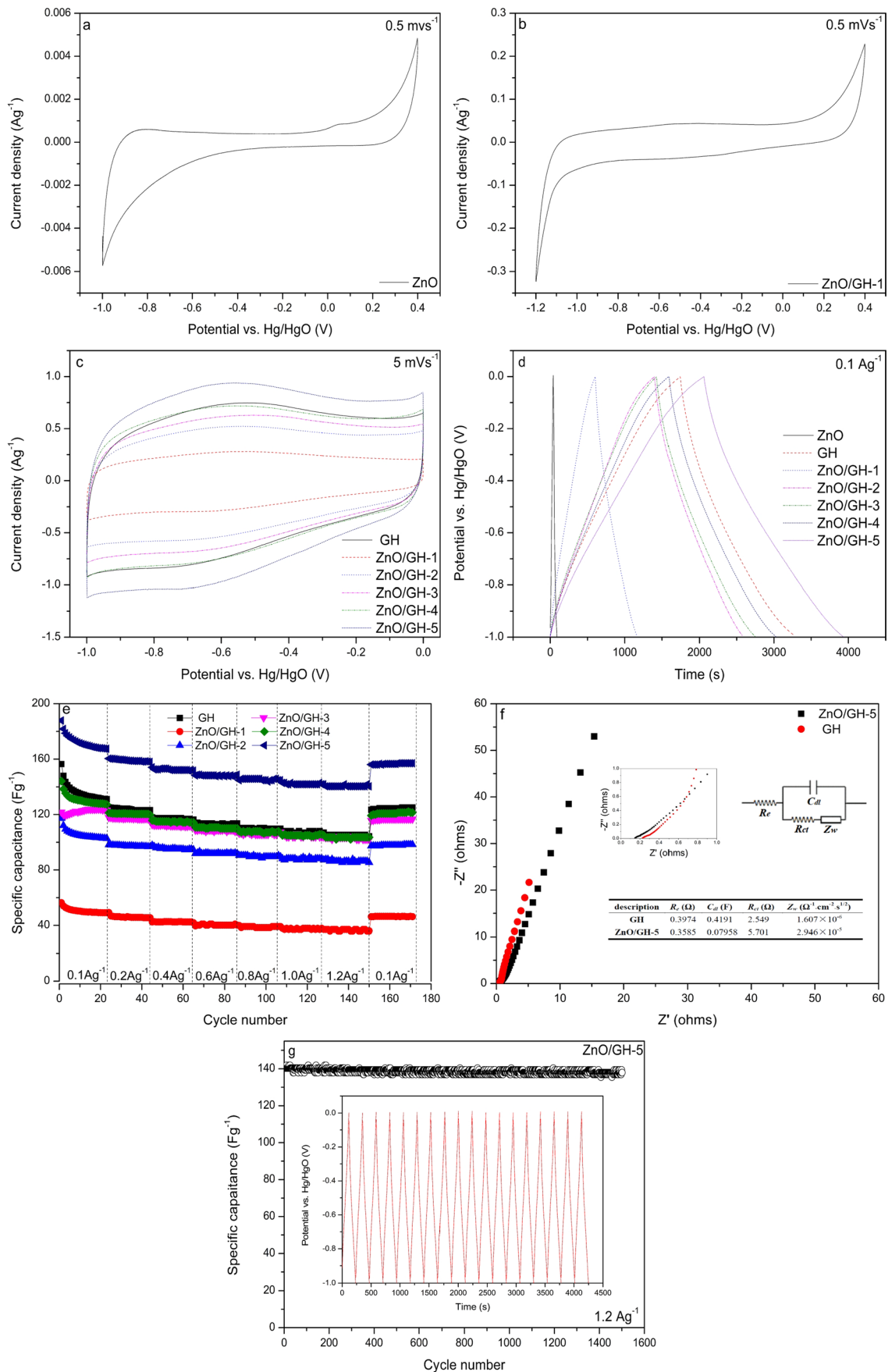


Fig. 6 CV curves of ZnO (a), ZnO/GH-1 nanocomposites (b), GH and ZnO/GH nanocomposites (c); GCD curves of GH and ZnO/GH nanocomposites (d); Rate performance of GH and ZnO/GH nanocomposites (e); Nyquist plots of GH and ZnO/GH nanocomposites (f). The inset is Nyquist plots in the high frequency area and its equivalent circuit diagram; Specific capacitance of ZnO/GH nanocomposites versus cycle number (g). The inset is the charge/discharge curves

restacked to diminish the BET surface area of GH during the reaction [32]. Then, ZnO nanorods deposited on the surfaces and edges of GH might separate the graphene layers as the spaces to increase the surface area of ZnO/GH-5 nanocomposites.

Figure 6a shows the CV curve of ZnO in the potential range from -1.2 to 0.4 V at 0.5 mVs $^{-1}$. On the curve, there are an oxygen evolution reaction at the scan potential above 0.10 V and another hydrogen evolution reaction at the potential under -0.40 V, owing to water decomposition reaction occurred in the KOH electrolyte. The curve shows an anodic peak at 0.05 V also, but the cathodic peak is invisible. In the potential range from -0.40 to 0.10 V, the ZnO CV exhibits a quasi-rectangular shape, indicating the obvious electric double layer feature. For a comparison purpose, the ZnO/GH-1 nanocomposites were tested by CV at the same testing condition. The CV curve (Fig. 6b) displays that H $_2$ evolution took place under -1.0 V and O $_2$ evolution above 0.0 V on the electrode, respectively. In the potential window from -1.0 to 0.0 V, there is a quasi-square shape of CV curve. The energy-storage principle of ZnO/GH-1 nanocomposites should be explained by the electrochemical double-layer capacitor [33].

The CV curves (Fig. 6c) of GH and ZnO/GH nanocomposites are all quasi-rectangular shapes in the potential range from -1.0 to 0.0 V at 5 mVs $^{-1}$. The shapes of curves indicate that the capacitance characteristics are mainly governed by the electric double layer. The specific capacitances of ZnO, GH, ZnO/GH-1, ZnO/GH-2, ZnO/GH-3, ZnO/GH-4, and ZnO/GH-5 nanocomposites can be calculated using Eq. (1):

$$C_s = I \times \Delta t / (m \times \Delta V) \quad (1)$$

where I is the constant discharge current (A), m is the mass of active materials in electrode (g), and Δt is the discharge time (s) in the potential window ΔV (V) [34]. According to their GCD curves (Fig. 6d) at 0.1 Ag $^{-1}$, the capacitances can reach 4.24 , 143.51 , 52.81 , 111.42 , 124.71 , 135.42 , and 187.88 Fg $^{-1}$, respectively. In addition, these curves exhibit almost straight lines, which further demonstrate good capacitive properties of as-prepared samples [35]. Combined with the TEM images (Fig. 4e–j) of nanocomposites, ZnO nanorods loaded on the surfaces of GH were found to agglomerate easily with an increase amount of Zn precursor. The agglomeration of nanorods greatly hinders

the interfacial contact between electrolyte and GH, resulting in a reduction in the effective surface area of GH for electrochemical double-layer formation. Hence, the as-prepared ZnO/GH nanocomposites could acquire the enhanced capacitance value with the decrease of ZnO mass.

For their practical applications, the rate capability and cycle stability of GH and ZnO/GH nanocomposites were studied through GCD techniques. After the electrodes continues 20 cycles at each of the current density (0.1 , 0.2 , 0.4 , 0.6 , 0.8 , 1.0 , and 1.2 Ag $^{-1}$) and then bring back to 0.1 Ag $^{-1}$ in the reverse order to run another 20 cycles as shown in Fig. 6e, it should be noted that the less ZnO is introduced, the higher specific capacitance of the as-prepared ZnO/GH nanocomposites has. The capacitance retention rates of GH, ZnO/GH-1, ZnO/GH-2, ZnO/GH-3, ZnO/GH-4, and ZnO/GH-5 nanocomposites are 86.03% , 87.61% , 87.36% , 92.88% , 88.08% , and 83.04% at 0.1 Ag $^{-1}$, respectively. The results indicate that samples have better reversibility for applying at higher charge/discharge rates. Their mechanisms of energy storage are inherently rapid because they simply involve movement of ions to and from electrode surfaces [36]. Figure 6g verifies the electrochemical stability of ZnO/GH-5 nanocomposites as an electrode material for supercapacitors at 1.2 Ag $^{-1}$. The retention of specific capacitance is 98.25% after 1500 cycles owing to a very high degree of reversibility based on an electric double layer mechanism.

Figure 6f depicts the Nyquist plots of GH and ZnO/GH-5 nanocomposites, which show the response of components performance in the frequency domain. In the low frequency range, two straight lines close to the imaginary axis indicate the pure capacitive behavior of samples [37]. The arcs and x -intercepts representing the very small charge transfer resistances and inner resistances of samples could be observed from the EIS curves in the high frequency region. For further confirmation, the plots have been analyzed on the basis of the equivalent circuit by the ZsimpWin software, which the circuit was comprised of the four elements: the solution resistance and interal resistance of the electrode (R_e), double-layer capacitance (C_{dl}), Warburg diffusion impedance (Z_w), and faradic charge transfer resistance (R_{ct}) [38]. As shown in the inset table of Fig. 5f, the R_e values of GH and ZnO/GH-5 composites are 0.3974 and 0.3585 Ω respectively. This displays that the ZnO/GH-5 nanocomposites have the lesser electrolyte resistance and maybe achieve larger specific capacitance, because it provides easier access to charge between electrode and electrolyte [27].

Conclusions

In summary, we have developed a two-step synthetic route to produce ZnO/GH nanocomposites. By XRD, FT-IR, SEM, and TEM analysis, the nanocomposites

have single-crystalline wurtzite structure. When a small amount of ZnO was formed on the surfaces of GH, they could restrict the agglomeration of GH to increase its surface area, in accordance with the results of N_2 adsorption/desorption tests. The as-prepared ZnO/GH nanocomposites all display the ideal capacitive behavior and fast charge-discharge behavior. The capacitance values of the samples increased in decreasing the ZnO mass. According to EIS testing results, the ZnO/GH-5 nanocomposites have smaller electrolyte resistance and electrode resistance. The material displayed an enhanced specific capacitance of 188 Fg^{-1} at 0.1 Ag^{-1} in the 6 M KOH solution, which was higher than pure GH (144 Fg^{-1}) and ZnO (4.24 Fg^{-1}). Additionally, it has also showed excellent cycling performance (98.25% after 1500 cycles at 1.2 Ag^{-1}). Therefore, the electrode material is a promising candidate for supercapacitors.

References

- Thiagarajan K, Theerthagiri J, Senthil RA, Arunackalam P, Madhavan J, Ghanem MA (2018) Synthesis of $Ni_3V_2O_8$ @graphene oxide nanocomposite as an efficient electrode material for supercapacitor applications. *J Solid State Electrochem* 22:527–536
- Novoselov KS, Geim AK, Morozov SV, Jiang D, Zhang Y, Dubonos SV, Grigorieva IV, Firsov AA (2004) Electric field effect in atomically thin carbon films. *Science* 306:666–669
- Lim TG, Suk JW (2021) Effect of the particle size of graphene oxide powders on the electrochemical performance of graphene-based supercapacitors. *Funct Compos Struct* 3:015005
- Theerthagiri J, Salla S, Senthil RA (2019) A review on ZnO nanostructured materials: energy, environmental and biological applications. *Nanotechnology* 30:27
- Ding FF, Zhang N, Zhang C (2015) Synthesis and electrochemical properties of functionalized graphene oxide/ZnO composites. *Eng Mater* 680:233–237
- Samuel E, Londhe PU, Joshi B, Kim MW (2018) Electrospayed graphene decorated with ZnO nanoparticles for supercapacitors. *J Alloys Compd* 741:781–791
- Miah M, Mondal TK, Ghosh A, Saha SK (2020) Study of highly porous ZnO nanospheres embedded reduced graphene oxide for high performance supercapacitor application. *Electrochim Acta* 354:136675
- Kumar R, Youssry SM, Abdei-Galei MM, Matsuda A (2020) One-pot synthesis of reduced graphene oxide nanosheets anchored ZnO nanoparticles via microwave approach for electrochemical performance as supercapacitor electrode. *J Mater Sci Mater Electron* 31:15456–15465
- Haldoral Y, Voit W, Shim JJ (2014) Nano ZnO@reduced graphene oxide composite for high performance supercapacitor: green synthesis in supercritical fluid. *Electrochim Acta* 120:65–72
- Zhang YP, Li HB, Pan LK, Lu T, Sun Z (2009) Capacitive behavior of graphene-ZnO composite film for supercapacitors. *J Electroanal Chem* 634(1):68–71
- Li XG, Wang ZK, Qiu YF, Pan QM, Hu PA (2015) 3D graphene/ZnO nanorods composite networks as supercapacitor electrodes. *J Alloys Compd* 620:31–37
- Samuel E, Londhe PU, Joshi B, Kim MW, Kim K, Swihart MT, Chauré NB, Yoon SS (2018) Electrospayed graphene decorated with ZnO nanoparticles for supercapacitors. *J Alloys Compd* 741:781–791
- Bu TYY, Huang R (2015) One-pot synthesis of ZnO/reduced graphene oxide nanocomposite for supercapacitor application. *Mater Sci Semicond Process* 31:131–138
- Subramani K, Sathish M (2019) Facile synthesis of ZnO nanoflowers/reduced graphene oxide nanocomposite using zinc hexacyanoferrate for supercapacitor applications. *Mater Lett* 236:424–427
- Du XX, Wang S, Liu YC, Lu MP, Wu K, Lu MG (2019) Self-assembly of free-standing hybrid film based on graphene and zinc oxide nanoflakes for high-performance supercapacitors. *J Solid State Chem* 277:441–447
- Ezeigwe ER, Tan MTT, Khiew PS, Siong CW (2015) One-step green synthesis of graphene/ZnO nanocomposites for electrochemical capacitors. *Ceram Int* 41:715–724
- Du GX, Wang XX, Zhang LD, Feng Y, Liu Y (2013) One-step green synthesis of graphene/ZnO nanocomposites. *Mater Lett* 98:168–170
- Wang GX, Yang J, Park J, Gou XL, Wang B, Liu H, Yao J (2008) Facile synthesis and characterization of graphene nanosheets. *J Phys Chem C* 112:8192–8195
- Szabó T, Berkesi O, Forgó P, Josepovits K, Sanakis Y, Petridis D, Dékány I (2006) Evolution of surface functional groups in a series of progressively oxidized graphite oxide. *Chem Mater* 18:2740
- Guo HL, Wang XF, Qian QY, Wang FB, Xia XH (2009) A green approach to the synthesis of graphene nanosheets. *ACS Nano* 3:2653–2659
- Gao XF, Jang JY, Nagase S (2010) Hydrazine and thermal reduction of graphene oxide: reaction mechanisms, product structures, and reaction design. *J Phys Chem C* 114:832–842
- Ambrozic G, Skapin SD, Zigon M, Orel ZC (2011) The formation of zinc oxide nanoparticles from zinc acrylate hydrate in tert-butanol: a comparative mechanistic study with isomeric C4 alcohols as the media. *Mater Res Bull* 46:2497–2501
- Petrovic Z, Ristic M, Music S, Fabian M (2015) Nano/microstructure and optical properties of ZnO particles precipitated from zinc acetylacetonate. *J Mol Struct* 1090:121–128
- Saranya M, Rajendran R, Wang F (2016) Graphene-zinc oxide (G-ZnO) nanocomposite for electrochemical supercapacitor applications. *J Sci Adv Mater Dev* 1:454–460
- Wu F, Xie AM, Sun MX, Wang Y, Wang MY (2015) Reduced graphene oxide (RGO) modified spongelike polypyrrole (PPy) aerogel for excellent electromagnetic absorption. *J Mater Chem A* 3:14358–14369
- Panigrahy B, Srivastava S (2016) Minuscule weight percent of graphene oxide and reduced graphene oxide modified Ag_3PO_4 : new insight into improved photocatalytic activity. *New J Chem* 40:3370–3384
- Matsuo Y, Iwasa K, Sugie Y, Mineshige A, Usami H (2010) Preparation of carbon-based transparent and conductive thin films by pyrolysis of silylated graphite oxides. *Carbon* 48:4009–4014
- Stankovich S, Dikin DA, Piner RD, Kohlhaas KA, Kleinhammes A, Jia YY, Wu Y, Nguyen ST, Ruoff RS (2007) Synthesis of graphene-based nanosheets via chemical reduction of exfoliated graphite oxide. *Carbon* 45:1558–1565
- Han W, Ren L, Qi X, Liu Y, Wei X, Huang Z, Zhang J (2014) Synthesis of Cd/ZnO/graphene composite with high-efficiency photoelectrochemical activities under solar radiation. *Appl Surf Sci* 299:12–18
- Zeng H, Cao Y, Xie X, Yang J, Tang Z, Wang X, Sun L (2013) Synthesis optical and electrochemical properties of ZnO nanowires/graphene oxide heterostructures. *Nanoscale Res Lett* 8:133

31. Hughesn M, Chen GZ, Shaffer MSP, Fray DJ, Windle AH (2002) Electrochemical capacitance of a nanoporous composite of carbon nanotubes and polypyrrole. *Chem Mater* 14:1610–1613
32. Lin ZY, Yao YG, Li Z, Liu Y, Li Z, Wong CP (2010) Solvent-assisted thermal reduction of graphite oxide. *J Phys Chem C* 114:14819–14825
33. Liao JJ, Li YJ, Wang ZY, Lv LF, Chang LP (2021) In-situ preparation of Fe₃O₄/graphene nanocomposites and their electrochemical performances for supercapacitor. *Mater Chem Phys* 258:123995
34. Qian W, Chen ZQ, Cottingham S, Merrill WA, Swartz NA, Goforth AM, Clare TL, Jiao J (2012) Surfactant-free hybridization of transition metal oxide nanoparticles with conductive graphene for high-performance supercapacitor. *Green Chem* 14:371–377
35. Kierzek K, Frackowiak E, Lota G, Gryglewicz G, Machnikowski J (2004) Electrochemical capacitors based on highly porous carbons prepared by KOH activation. *Electrochim Acta* 49:515–523
36. Wakeland S, Martinez R, Grey JK, Luhrs CC (2010) Production of graphene from graphite oxide using urea as expansion-reduction agent. *Carbon* 48:3463–3470
37. Pandolfo AG, Hollenkamp AF (2006) Carbon properties and their role in supercapacitors. *J Power Sources* 157:11–27
38. Ghosh A, Miah M, Majumder C, Bag S, Chakravorty D, Saha SK (2018) Synthesis of multilayered structure of nano-dimensional silica glass/reduced graphene oxide for advanced electrochemical applications. *Nanoscale* 10:5539

Publisher's note Springer Nature remains neutral with regard to jurisdictional claims in published maps and institutional affiliations.